

Trends in **Applied Sciences** Research

ISSN 1819-3579



The Effect of Frequency on the Cyclic Strain Accumulation of Plain Stainless Steel Pressurized Cylinders Subjected to Dynamic Bending Moment

¹S.J. Zakavi, ¹M. Zehsaz and ²M.R. Eslami ¹Faculty of Mechanical Engineering, University of Tabriz, Tabriz, Iran ²Faculty of Mechanical Engineering, Amirkabir University of Technology, Tehran, Iran

Abstract: The aim of this study is to evaluate the effect of frequency on the ratchetting behavior of plain stainless steel pressurized cylinders that may be used in the power plant components. The cylinder is subjected to an internal pressure (calculated as the design pressure for each cylinder) and alternately bending moments at different frequencies typical of seismic events. Ratchetting of the cylinder wall has been observed and recorded in the hoop direction. The nonlinear isotropic/kinematic (combined) hardening model is used to evaluate the ratchetting. Finite element analysis which models the cylinders under above mentioned loads and combined hardening model is applied to investigate the ratchetting. Stress-strain data and material parameters have been obtained from several stabilized cycles of specimens that are subjected to symmetric strain cycles. The results show that initially, the calculated rate of ratchetting is large and then decreases with the increasing of cycles. Also, the ratchetting data using FE analysis show the hoop strain ratchetting decreases with the increasing of frequencies and spacing from the resonant frequency.

Key words: Ratchetting, pressurized pipes, cyclic bending moment, frequency, strain hardening, finite element

INTRODUCTION

The literature review shows that accurate closed form solutions may not be found to analyze the ratchetting behavior of the pressurized pipes under cyclic bending loading which can be caused by seismic loads. However, approximate solutions have been developed by Cao et al. (2009), Tasnim et al. (2008), Rahman et al. (2008), Zehsaz et al. (2008), Chaboche (1989, 1991, 1994, 2008), Abdel-Karim (2005) Chen et al. (2005), Johansson et al. (2005), Chen and Jiao (2004), Bari and Hassan (2001, 2002), Abdel-Karim and Ohno (2000) and Beaney (1990, 1991) which can be used to calculated the induced incremental plastic strains caused by ratchetting. Experimental works to study the ratchetting of the straight pipes have also been carried out by the EPRI (Ranganath et al., 1989; English, 1988).

The kinematic hardening theory of plasticity based on the Armstrong-Frederick model is used to evaluate the cyclic loading behavior of thick cylindrical vessels. The results found from their numerical analysis shows that the when the stress range is more than twice the yield stress, kinematic hardening theory with the Armstrong-Frederick model excluding creep,

Corresponding Author: S.J. Zakavi, Faculty of Mechanical Engineering, University of Tabriz, Tabriz, Iran Tel: +98 914 151 2877 Fax: +98 451 551 2904 predicts ratchetting for load controlled cyclic loading while shakedown is predicted for deformation controlled cyclic loading. Kinematic hardening theory with the Prager model predicts shakedown for load and deformation controlled cyclic loading of thick vessels (Eslami and Mahbadi, 2001).

The study reported here is based on a series of tests conducted using specimens having $D_m/t = 12$. There is notable dearth of information available which seeks to compare experimental data such as that reported by Moreton *et al.* (1994, 1996, 1998a, b) with finite element computations. This is surprising since it is well known that analytical solutions, (such as those presented in references (Beaney, 1990), differ with experimental data by several orders of magnitude. It is of paramount importance to establish reliable theoretical methods for predicting ratchetting rates and the use of Finite Element (FE) codes would seem to be a logical way forward. Therefore, in this study a finite element analysis with the nonlinear isotropic/kinematic (combined) hardening model is used to evaluate ratchetting behavior of plain stainless steel pressurized cylinders subjected to dynamic bending moment with different frequency.

MATERIALS AND METHODS

In this study, a finite element code, ABAQUS, is used to study the effect of frequency on the ratchetting of plain stainless steel pressurized pipes subjected to cyclic bending loading. First, a series of tests have been undertaken subjecting the pressurized pipe specimens to rising amplitude dynamic bending moments at the resonant frequency of about 5 Hz to simulate a seismic event. Generally, the fundamental (resonant) frequency of piping system is low (typically less than 5 Hz), due to the necessity of flexibility to cope with thermal loads (Touboul *et al.*, 2006). Second, by conducting a series of finite element runs based on the nonlinear isotropic/kinematic hardening model using the ABAQUS, the experimental tests are modeled and ratchetting data obtained. The two sets of results are compared with each other.

Also, in this study, the effect of frequency on the ratchetting behavior of plain stainless steel pressurized cylinders used in the power plant components is investigated.

HARDENING MODEL

The isotropic and kinematic hardening models are used to simulate the inelastic behavior of materials that are subjected to cyclic loading. The use of plasticity material models with isotropic type hardening is generally not recommended since they continue to harden during cyclic loading. The isotropic hardening model always predicts shakedown behavior, if creep is not considered. The kinematic hardening plasticity models are proposed to model the inelastic behavior of materials that are subjected to repeated loading. For example, the Armstrong-Frederick kinematic hardening model is suggested for the nonlinear strain hardening materials. The results of these models are discussed for structures under various types of cyclic loads in references (Rahman *et al.*, 2008; Eslami and Mahbadi, 2001; Prager, 1956).

A kinematic hardening model or a (combined) nonlinear isotropic/kinematic hardening model may be used to simulate the behavior of materials that are subjected to cyclic loading. The evolution law in these models consists of a kinematic hardening component which describes the translation of the yield surface in the stress space. An isotropic component which describes the change of the elastic range is added for the nonlinear isotropic/kinematic hardening model.

Isotropic Hardening Model

The isotropic hardening model which describes the change of the elastic range is discussed here. The isotropic hardening means that the yield surface changes size uniformly in all directions such that the yield stress increases in all stress directions as plastic straining occurs.

According to the isotropic hardening rule, the evolution of the loading surface is governed only by one scalar variable, R. For time independent plasticity and isothermal plastic deformation, the yield surface is expressed as (Lemaitre and Chaboche, 1994):

$$f = f(\sigma, R)$$
 (1)

The above equation, considering the von-Misses criterion may be rewritten in the form (Chaboche, 1989):

$$f = J_{\gamma}(\sigma) - R - k \tag{2}$$

where, k is the initial size of the yield surface and R is the isotropic hardening parameter that can be expressed as a function of the equivalent plastic strain ε_P :

$$R = R (\varepsilon_p) \tag{3}$$

with ε_{P} defined through:

$$d\varepsilon_p = \sqrt{\frac{2}{3}}d\varepsilon^p : d\varepsilon^p$$
(4)

and J₂ denotes the von-Mises distance in the deviatoric stress space:

$$J_2(\sigma) = \sqrt{\frac{3}{2}\sigma' : \sigma'}$$
(5)

where σ and σ' are the stress and stress deviatoric tensors in the stress space.

The flow rule associated with the yield function has the general form (Lemaitre and Chaboche, 1994):

$$d\epsilon^{P} = d\lambda \frac{\partial f}{\partial \sigma} = \frac{3}{2} d\lambda \frac{\sigma'}{R + k}$$
 (6)

where, the constant $d\lambda$ is defined as $d\lambda = d\epsilon_p$.

The isotropic hardening can be introduced using the evolution of the size of the yield surface as (Chaboche, 1989):

$$dR = b(Q-R)d\varepsilon_{P} \tag{7}$$

where, Q and b are two material coefficients. Integrating the above equation with the initial value R = 0 gives:

$$R = Q(1 - e^{ab\epsilon_p}) \tag{8}$$

Kinematic Hardening Model

The classical linear kinematic hardening rule and different nonlinear kinematic hardening models are available for the plastic analysis of structures. The nonlinear kinematic hardening model was first proposed by Armstrong and Frederick (1966). Nonlinearities are given as a recall term in the Prager rule. So, that the transformation of yield surface in the stress space is different during loading and unloading. This is done by assuming different hardening modulus in loading and unloading conditions.

The yield function for time independent plasticity, using the von-Mises yield criterion, is expressed as (Lemaitre and Chaboche, 1994):

$$f = J_2 (\sigma - X) - k \tag{9}$$

where, X is the back stress tensor, k is the initial size of the yield surface and J₂ denotes the von-Mises distance in the deviatoric stress space:

$$J_{2}(\sigma - X) = \left[\frac{3}{2}(\sigma' - X') : (\sigma' - X')\right]^{\frac{1}{2}}$$
 (10)

where, σ and X are the stress and back stress tensors and σ' and X' are the stress and back stress deviatoric tensors in the stress space, respectively.

The nonlinearities are given as a recall term in the Prager rule:

$$dX = \frac{2}{3}Cd\varepsilon^{P} - \gamma X d\varepsilon_{P}$$
 (11)

where, $d\epsilon_P$ is the equivalent plastic strain rate, C and γ are two material dependent coefficients in the Armstrong-Frederick kinematic hardening model and $\gamma = 0$ stands for the linear kinematic rule.

The normality hypothesis and the consistency condition df = 0 lead to the expression for the plastic strain rate (Lemaitre and Chaboche, 1994):

$$d\epsilon^{P} = d\lambda \frac{\partial f}{\partial \sigma} = \frac{H(f)}{h} \left\langle \frac{\partial f}{\partial \sigma} : d\sigma \right\rangle \frac{\partial f}{\partial \sigma}$$
(12)

where, H denotes the Heaviside step function: H(f) = 0 if f < 0, H(f) = 1 if $f \ge 0$ and the symbol $\langle \rangle$ denotes the MacCauley bracket, i.e., $\langle u \rangle = (u + |u|)/2$.

The hardening modulus h becomes:

$$h = C - \frac{3}{2}\gamma X : \frac{\sigma' - X'}{k} \tag{13}$$

In the case of tension-compression, the criterion and the equations of flow and hardening can be expressed in the form (Lemaitre and Chaboche, 1994):

$$f = |\sigma - X| - k = 0 \tag{14}$$

Trends Applied Sci. Res., 4 (4): 200-215, 2009

$$d\varepsilon_{p} = \frac{1}{h} \left\langle \frac{\sigma - X}{k} d\sigma \right\rangle \frac{\sigma - X}{k} = \frac{d\sigma}{h}$$
 (15)

$$dX = C d\varepsilon_p - \gamma X |d\varepsilon_p| \qquad (16)$$

$$h = C - \gamma X \operatorname{Sgn}(\sigma - X) \tag{17}$$

The evolution equation of hardening can be integrated analytically to give:

$$X = v \frac{C}{\gamma} + (X_0 - v \frac{C}{\gamma}) \exp[-v \gamma (\varepsilon_p - \varepsilon_{p_0})]$$
 (18)

where, $v = \pm 1$ according to the direction of flow and ϵ_{p_0} and X_0 are the initial values. For example at the beginning of each plastic flow.

Nonlinear Isotropic/Kinematic (Combined) Hardening Model

In the kinematic hardening models, the center of the yield surface moves in the stress space due to the kinematic hardening component. In addition, when the nonlinear isotropic/kinematic hardening model is used, the yield surface range may expand due to the isotropic component. These features allow modeling of inelastic deformation in metals that are subjected to cycles of load or temperature, resulting in significant inelastic deformation and, possibly, low-cycle fatigue failure.

The evolution law of this model consists of two components: a nonlinear kinematic hardening component, which describes the translation of the yield surface in the stress space through the back stress X and an isotropic hardening component, which describes the change of the equivalent stress defining the size of the yield surface R as a function of plastic deformation.

The kinematic hardening component is defined to be an additive combination of a purely kinematic term (linear Ziegler hardening law) and a relaxation term (the recall term), which introduces the nonlinearity. When temperature and field variable dependencies are omitted, the hardening law is:

$$dX = C \frac{1}{R} (\sigma - X) d\epsilon_p - \gamma X d\epsilon_p \qquad (19)$$

where, C and γ are the material parameters that must be calibrated from the cyclic test data. Here, C is the initial kinematic hardening modulus and γ determines the rate at which the kinematic hardening modulus decreases with increasing the plastic deformation. The kinematic hardening law can be separated into a deviatoric part and a hydrostatic part; only the deviatoric part has an effect on the material behavior. When C and γ are zero, the model reduces to an isotropic hardening model. When γ is zero, the linear Ziegler hardening law is recovered.

The isotropic hardening behavior of the model defines the evolution of the yield surface size R as a function of the equivalent plastic strain ε_p . This evolution can be introduced by specifying R as a function of ε_p by using the simple exponential law:

$$R = k + Q(1 - e^{-b\varepsilon_p})$$
 (20)

where, k is the yield stress at zero plastic strain and Q and b are the material parameters. Here, Q is the maximum change in the size of the yield surface and b defines the rate at which the size of the yield surface changes as plastic straining develops. When the equivalent stress defining the size of the yield surface remains constant (R = k), the model reduces to a nonlinear kinematic hardening model.

REVIEW OF EXPERIMENTAL ARRANGEMENT

The experimental arrangements used for testing plain cylinders and other pressurized piping components have been detailed previously (Moreton et al., 1998a). It is sufficient to give a brief outline of the technique.

Cylindrical specimens were machined from stainless steel bar stock to the form illustrated in Fig. 1. In order to minimize any residual stresses, these specimens were machined 1.5 mm oversize on all dimensions. These blanks were stress relived at 650°C (1 h + furnace cool). The bores of all specimens were reamed to 30 mm diameter and the outside surface profiled using a CNC (computer numeric controlled) lathe while holding the specimen on a mandrel. Six holes were provided in each end flange using the powered axial tooling of the CNC lathe. The specimens were machined in this way and the dimension A is given in Table 1.

Strain gauges were bonded to the top and bottom surfaces using M-Bond AE 10 curing for 4 h at 30°C and 2 h at 100°C. Two-element, 90 rosettes were used to provide strain measurement in the hoop and axial directions. The gauge type selected was EA-06-125TM-120 from Micro measurements.

Tensile test specimens were taken axially from the bar stock. These were subjected to the same oversize machining, heat treatment and final machining stages as the cylindrical specimens. Tensile test showed that the linear part of the curve extended up to about 180 MPa and then strain-hardened significantly up to 76% strain with an ultimate stress of 565 MPa. Using the ASME III, Boiler and Pressure Vessel Code (section III, subsection NB), the allowable design stress intensity S_m was determined as:

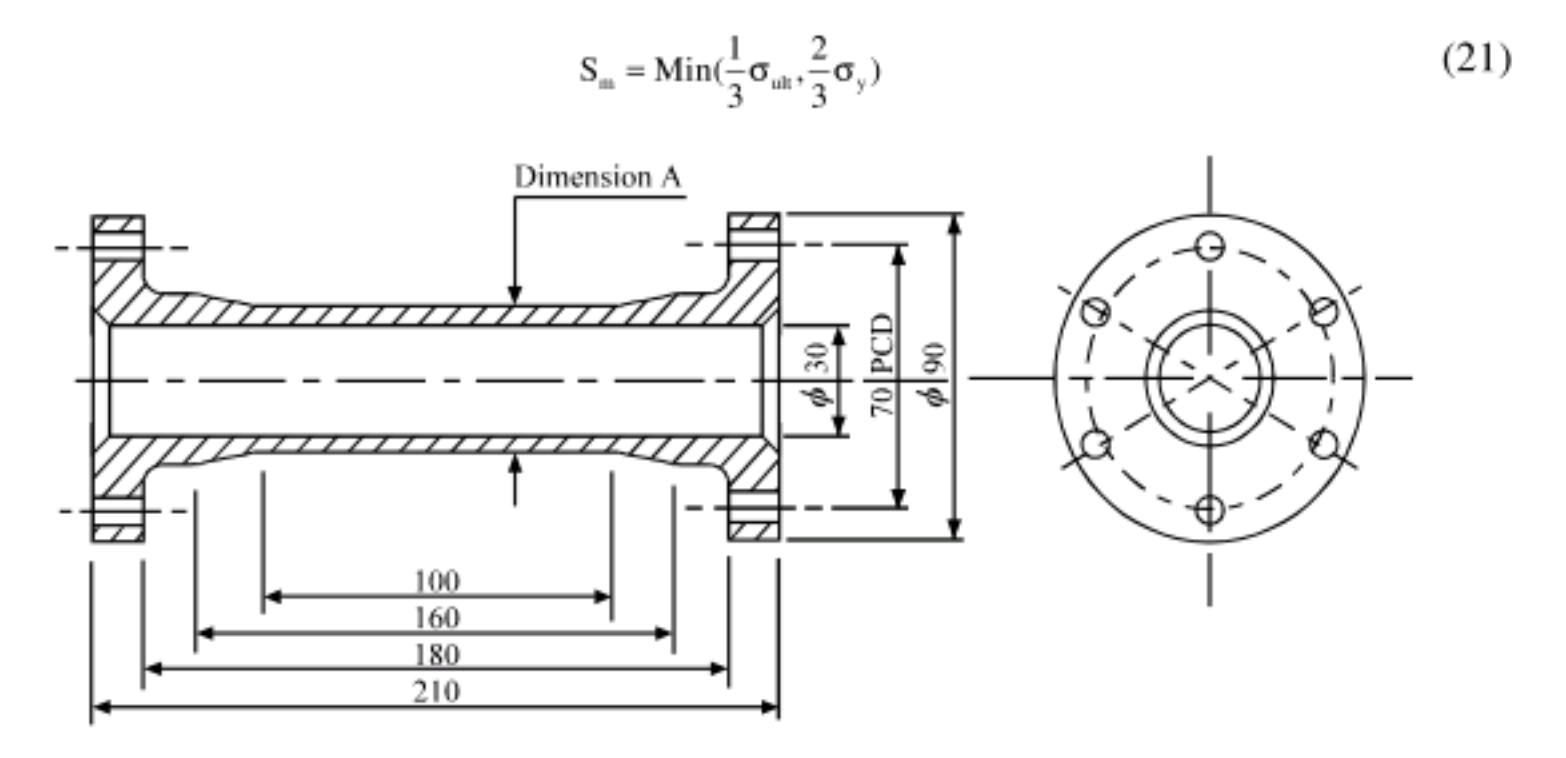


Fig. 1: The test specimen-All dimensions in mm

Table 1: Specimen SS with $D_m/t = 12$

ruote it opeennen oo t	THE PART IS		
Specimen	Dimension A (mm)	t (mm)	D _m /t
SS	35.46	2.73	12

A typical stress-strain curve is included in Fig. 2. It should be noted that all values of stress given above and in Fig. 2 are engineering stress. The rig used to provide simulated seismic bending is illustrated in Fig. 3. This is a 250 kN servo hydraulic testing machine fitted with a fatigue module. The test specimen was attached to extension limbs (via the flanged connections) and mounted in roller bearing supports outboard of the flanged connections. Tuning weights were added to the ends of the extension limbs which were supported on constant force springs to eliminate any gravity stresses. Excitation of the test machine cross head thus caused large-amplitude vibration of the test pipe work. Frequency sweeps at elastic amplitudes allowed the natural frequency to be established and to confirm the

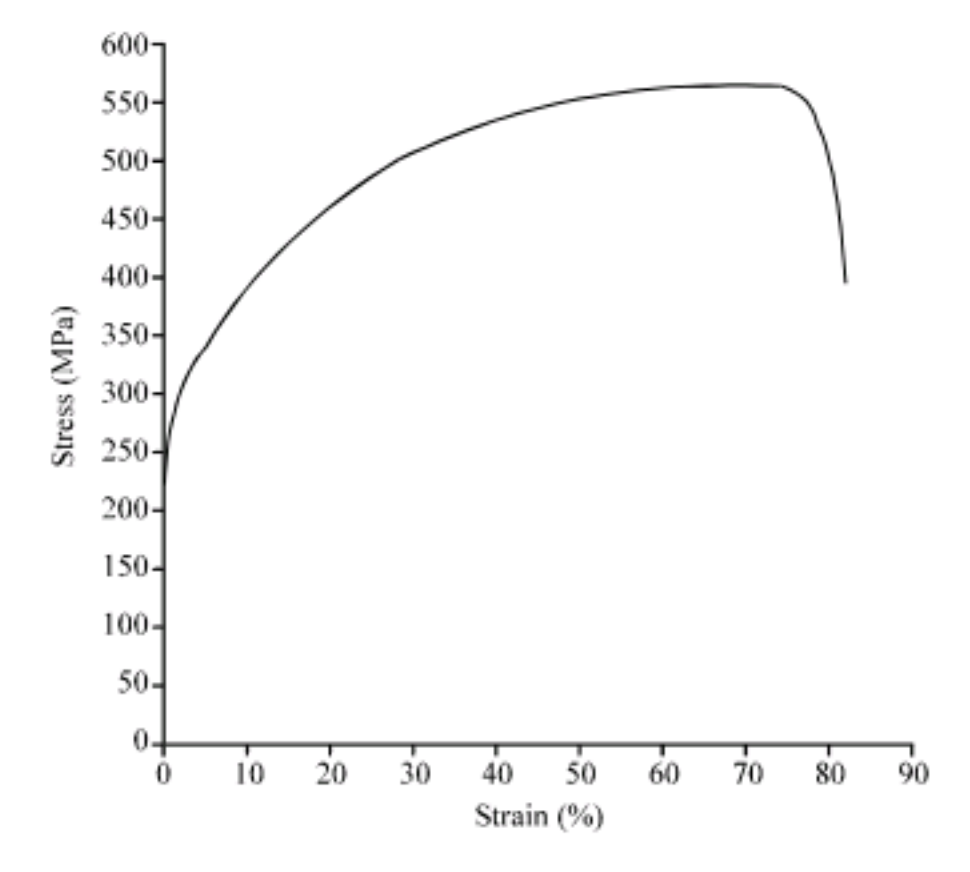


Fig. 2: Stress-strain curve for the stainless steel used to manufacture the tubular specimens

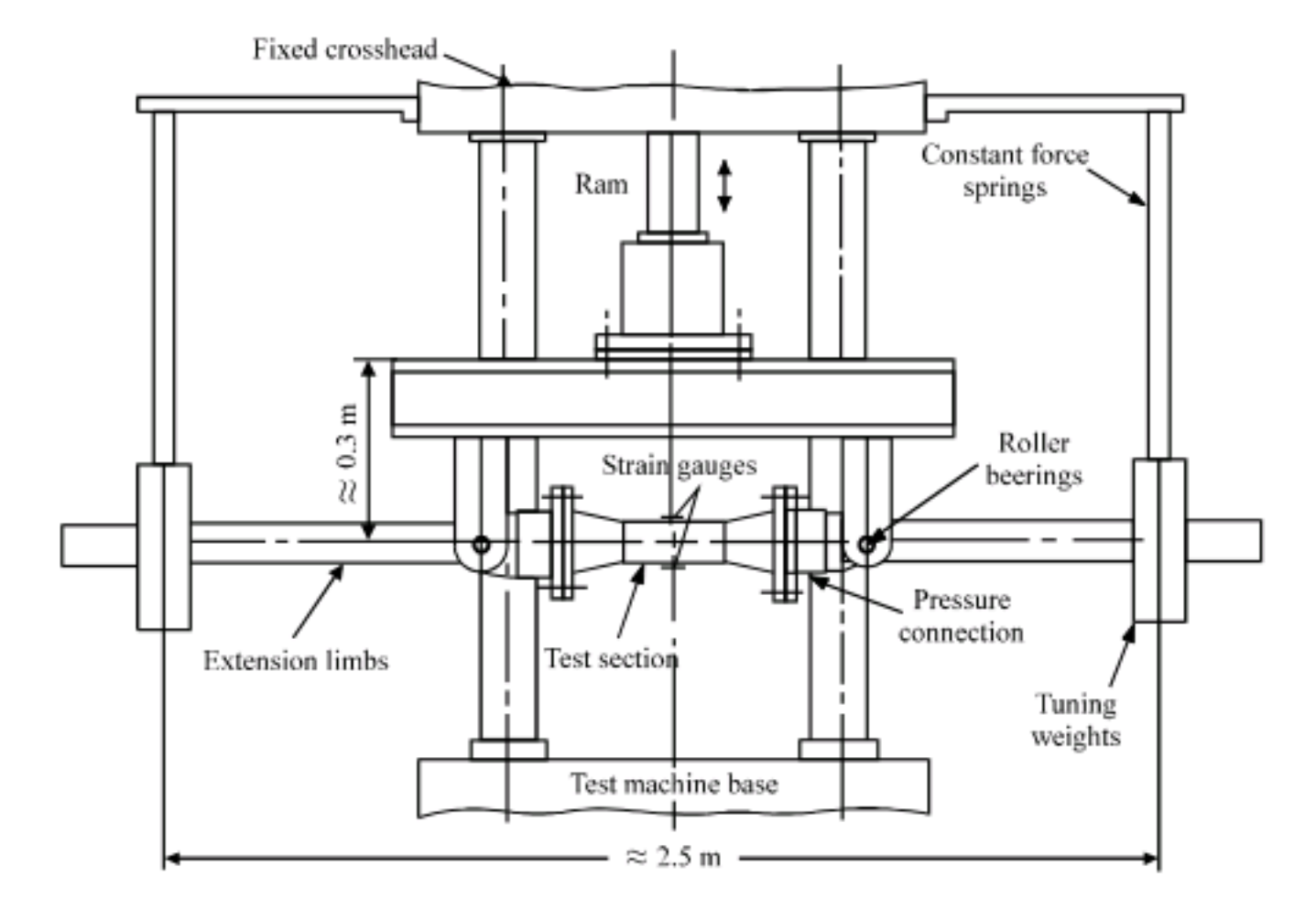


Fig. 3: The seismic test rig (Moreton et al., 1998b)

amplitude of vibration to be the same on each side of the rig. The bending moment experienced by the test specimen was extrapolated from moment measurements made in the elastic region of the extension limbs.

The design pressure for each cylinder was calculated using the ASME III code, which gives:

$$P_d = \frac{2S_m t}{D_n - 2yt}$$
(22)

With $S_m = 161$ MPa (Table 2) and y = 0.4.

All specimens were tested using a rising amplitude technique; i.e., having mounted the specimen in the test rig, tuned the natural frequency and applied the test pressure, where small input amplitude was applied and maintained for about 20 sec. During this time a high-speed data logger was used to record the input displacement, all strain gauge readings and the output acceleration provided by an accelerometer positioned on one of the tuning weights. Having completed such a test, the amplitude of vibration was increased and the process repeated. At high input amplitudes the duration of the test was reduced because of the limited stored hydraulic capacity of the testing machine.

FINITE ELEMENT ARRANGEMENT

For all specimens the nonlinear finite element code, ABAQUS, was used to study ratchetting of straight pressurized pipe subjected to simulated seismic bending moments.

The cylindrical specimen model under pressure and cyclic bending moment is shown in Fig. 4. The simulation assembly was a 2.30 m long pipe work modeled by 23 elements. The central test section was 3 elements long and the lateral extension limbs 10 elements long. Each element used 18 integration points around the pipe and four Fourier (or ovalization) modes. In the radial direction, 7 and 9 integration points through the thickness were used for the thin- and thick-walled models, respectively. The latter numbers of integration points were decided after a series of solution convergence runs. In the analysis, the load reactions were

 Table 2: Material properties obtained by tensile test

 Properties
 Value

 Young's modulus
 200 GPa

 Ultimate stress
 565 MPa

 2% proof stress
 242 MPa

 Elongation at failure (%)
 81%

 $S_m = \min (\sigma_{uh}/3, 2\sigma_{s}/3)$ 161 MPa

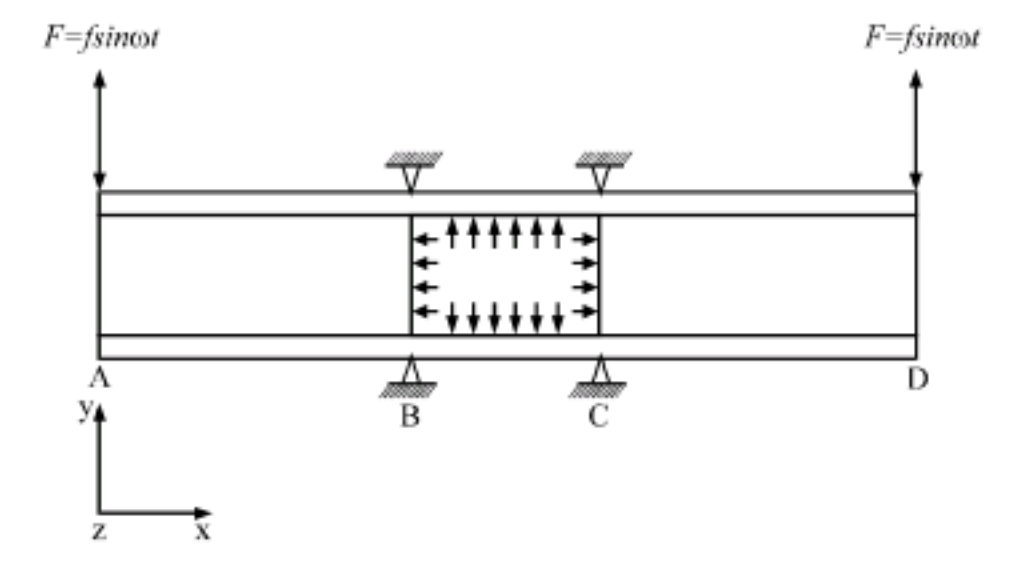


Fig. 4: Cylindrical specimen model under pressure and cyclic bending moment

simulated by applying boundary conditions at nodes 11 and 14 of the model. The latter nodes are the ends of the three elements making up the central test section. The displacements in all three directions and twisting about the pipe axis were prevented at these nodes. The additional boundary condition along the pipe axis was to simulate the closed end axial force reaction due to the internal pressure.

The most accurate element in the ABAQUS code for this type of structural system considering beam elements, pipe elements and elbow elements is the elbow element. Four types of elbow elements are available in the ABAQUS library, of which the two-noded element ELBOW 31B was found to give the best results. Although, these elbow elements appear like beam elements, they are actually elements where shell theory is used to model the behavior. Element type ELBOW 31B is cheaper (in computational time) than the standard ELBOW 31 and ELBOW 32 elements. It uses a simplified formulation where only ovalization is considered. Both warping and axial gradients of the ovalization are neglected.

The loading was applied in two stages. First the internal pressure, set at the design value of the pipe, was applied and held constant for the remainder of the analysis. Next, the dynamic load to induce the cyclic bending was applied at the end nodes of the simulation model. It was specified as a sinusoidal force with a circular frequency as obtained from the simulation test. Because of the dynamic nature of the analysis which induces different inertia loads due to the distributed weight of the lateral extension limbs as the vertical displacement frequency and amplitude were increased, the amplitude of the excitation had to be carefully adjusted until an equivalent moment equal to the value obtained during testing was achieved.

The material parameters of the kinematic hardening component of the model C = 1488.77 MPa, $\gamma = 6.15$ and the cyclic hardening parameters of the isotropic hardening component Q = 123.87 MPa and b = 1.98 are calibrated from test data obtained from several stabilized cycles by the exponential law.

EXPERIMENTAL AND FE RESULTS

Detailed results will be presented for specimen SS. It is perhaps useful to present, firstly, the bending moment response obtained by the FE analysis (Fig. 5). This clearly shows that a reasonably stable bending moment response has been achieved for the duration of the test.

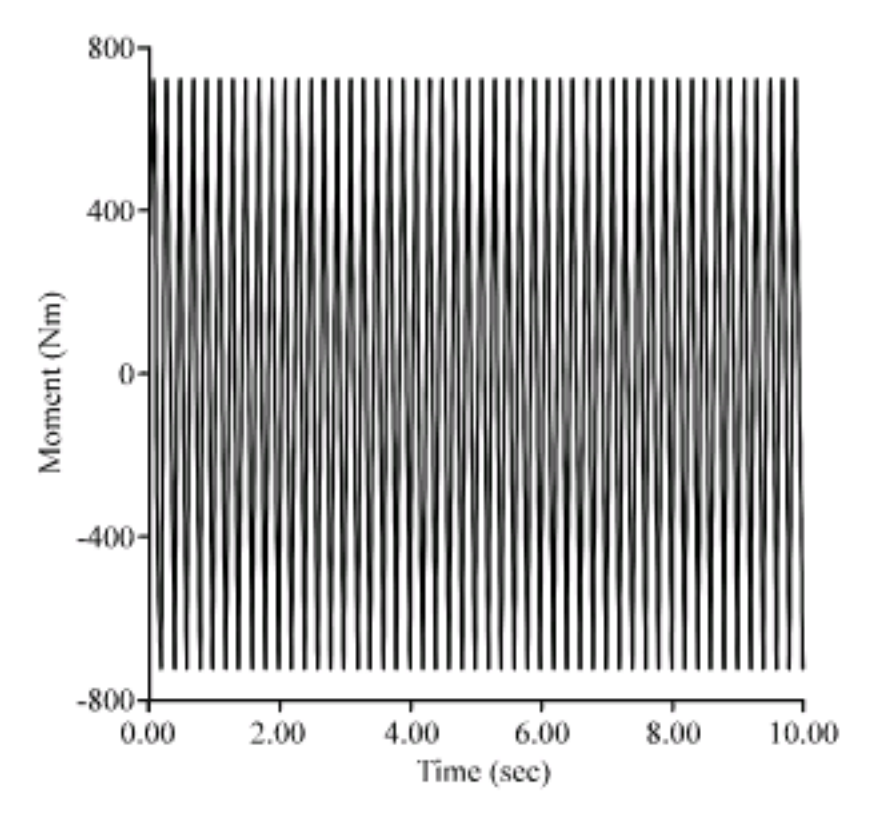


Fig. 5: FE analysis dynamic bending moment responses for the specimen SS at M=724.10 Nm and Frequency = 5.00 Hz

Strain gauges and a high-speed data capture system were used to record the experimental hoop and axial strains developed on the top and bottom surfaces of the seismic specimens. A FORTRAN routine was written to reconstruct the form of the strain signal. The experimentally obtained axial strain was found to be constant throughout the test and thus no data for these gauges has been included.

The results for specimen SS is shown in Fig. 6, which includes results from the FE analysis using with the combined hardening model. Here, the ratchet strain per cycle averaged over the first 20 sec of excitation has been plotted against increasing $M/M_{0.2}$ ratios for the experimentally obtained data and the finite element data ($M_{0.2}$ is moment based on proof stress $\sigma_{0.2}$ = 242 MPa). For both experimental data and the finite element results, the averages of the top and bottom surface ratchet strains are shown.

It is evident from Fig. 6 that the hoop strain ratcheting rates predicted by the FE analysis is near that found experimentally in all cases that $M/M_{P0.2} \le 1$. Otherwise, the results show that the FE method gives over estimated values comparing with the experimental data.

The response of the specimens during these tests is illustrated in Fig. 7. The dynamic bending moment experienced by the specimen has been plotted against the input displacement for the specimen SS. Although, there is some evidence in this plot that the dynamic bending moments do approach a self-limiting value, this is much less distinct than has been seen in previous works (Moreton *et al.*, 1996; Beaney, 1990).

Swelling introduced by ratcheting for stainless steel is shown in Fig. 8. This Fig. 8 shows the nature of this failure for typical specimen of stainless steel which appears to be a combination of hoop ratcheting (leading to the gross local swelling of the cylinder) and fatigue causing the hoop crack.

In Table 3, the ratchet strains found experimentally over a 20 sec test period and by FE analysis, for the same period, for specimen SS are summarized. The strains recorded on the top and bottom surfaces were found to be significantly different. In Table 3, the average of these two surface strains is presented. The effect of frequency on the ratchet strains is presented in Table 4, 5 and is shown in Fig. 9, 10. For specimen SS, the resonant frequency

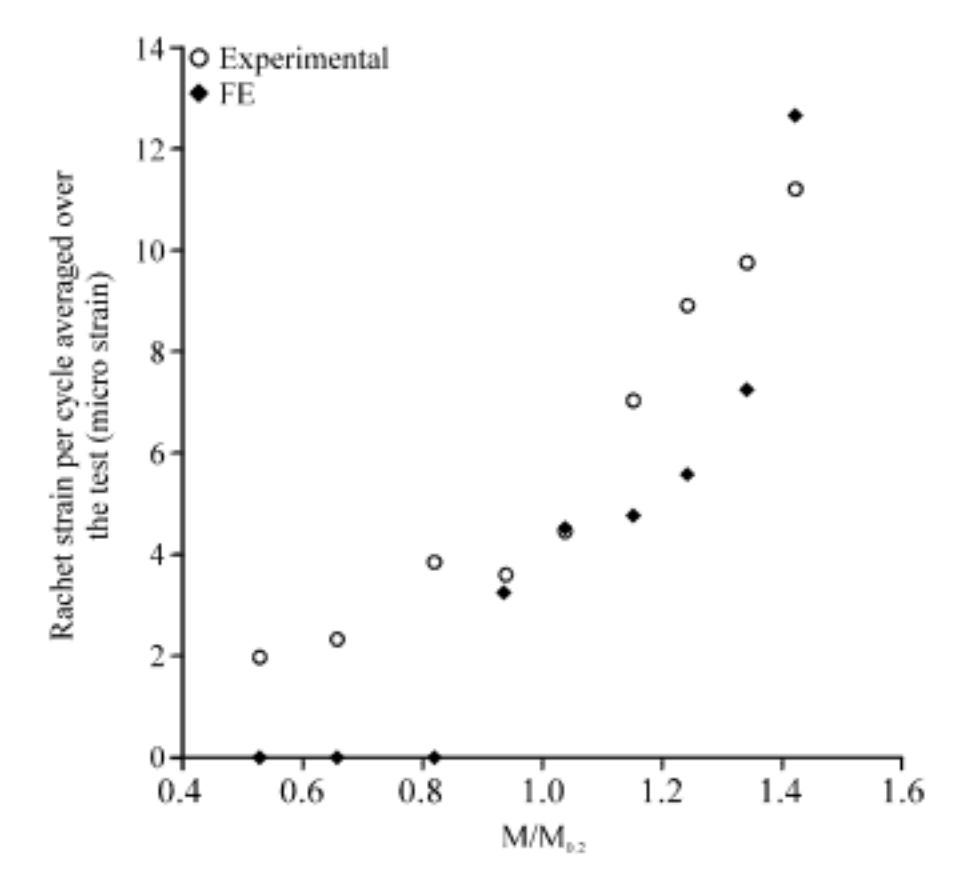


Fig. 6: Experimental and FE (combined hardening) ratchet strains for specimen SS at a testing frequency of 7.26 Hz

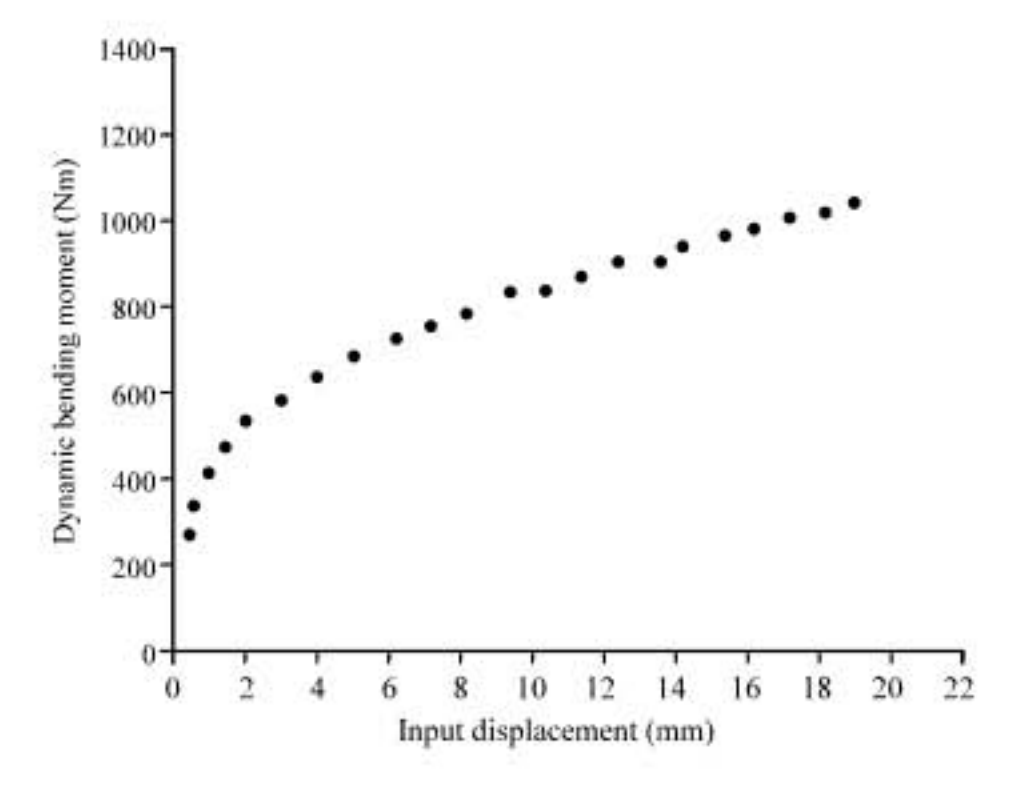


Fig. 7: Dynamic bending moment against the input displacement for the specimen SS

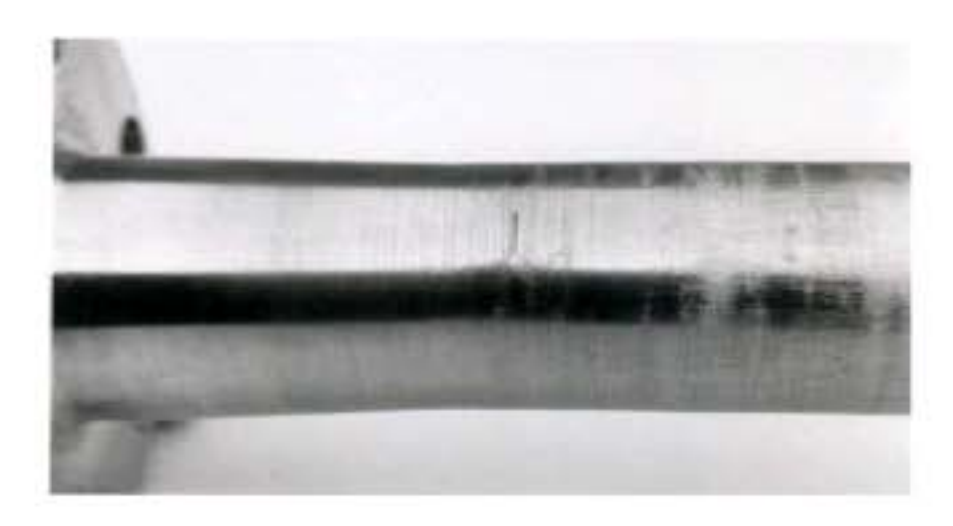


Fig. 8: Swelling in stainless steel specimen

Table 3: Experimental and FE ratchetting data for specimen SS

Dynamic bendi moment	ng M/M _{0.2}	$M/M_{P0.2}$	Experimental ratchet rate averaged over the test (µɛ/cycle)	FE (combined) ratchet rate averaged over the first 20 sec (με/cycle)
271.45	0.53	0.39	1.99 (20)	0
334.95	0.66	0.48	2.35 (20)	0
415.25	0.82	0.60	3.88 (20)	0
475.25	0.94	0.68	3.56 (20)	3.23
530.60	1.04	0.76	4.44 (20)	4.53
582.45	1.15	0.84	7.04 (20)	4.77
632.45	1.24	0.91	8.89 (19.15)	5.56
680.10	1.34	0.98	9.73 (17.77)	7.20
724.10	1.42	1.04	11.24 (16.39)	12.64
784.00	1.54	1.13	18.82 (8.95)	61.84

Columns 4, 5 are the average of the top and bottom surface strains. Data obtained for P = Pd = 26.10 Mpa $(P/P_{0.2} = 0.66)$. $M_{0.2}$ was based on proof stress $\sigma_{0.2} = 242$ MPa. Values in parentheses in column five indicate the duration of the test in seconds at a testing frequency of 7.26 Hz

is about 5 Hz. In Table 3 by increasing the dynamic bending moment in constant frequency, it considers that the hoop strain ratchet rate increase. The ratchet strain per cycle averaged over the test has been plotted against increasing frequency for the finite element data and is shown in Fig .10. Also, the results of FE analysis in Table 4 show that when the bending moment is constant then the hoop strain ratchet rate decreases with the increasing of the frequency. In the higher dynamic bending moments and in the frequency near the resonant frequency value, it considers that the hoop strain ratchet rate is more.

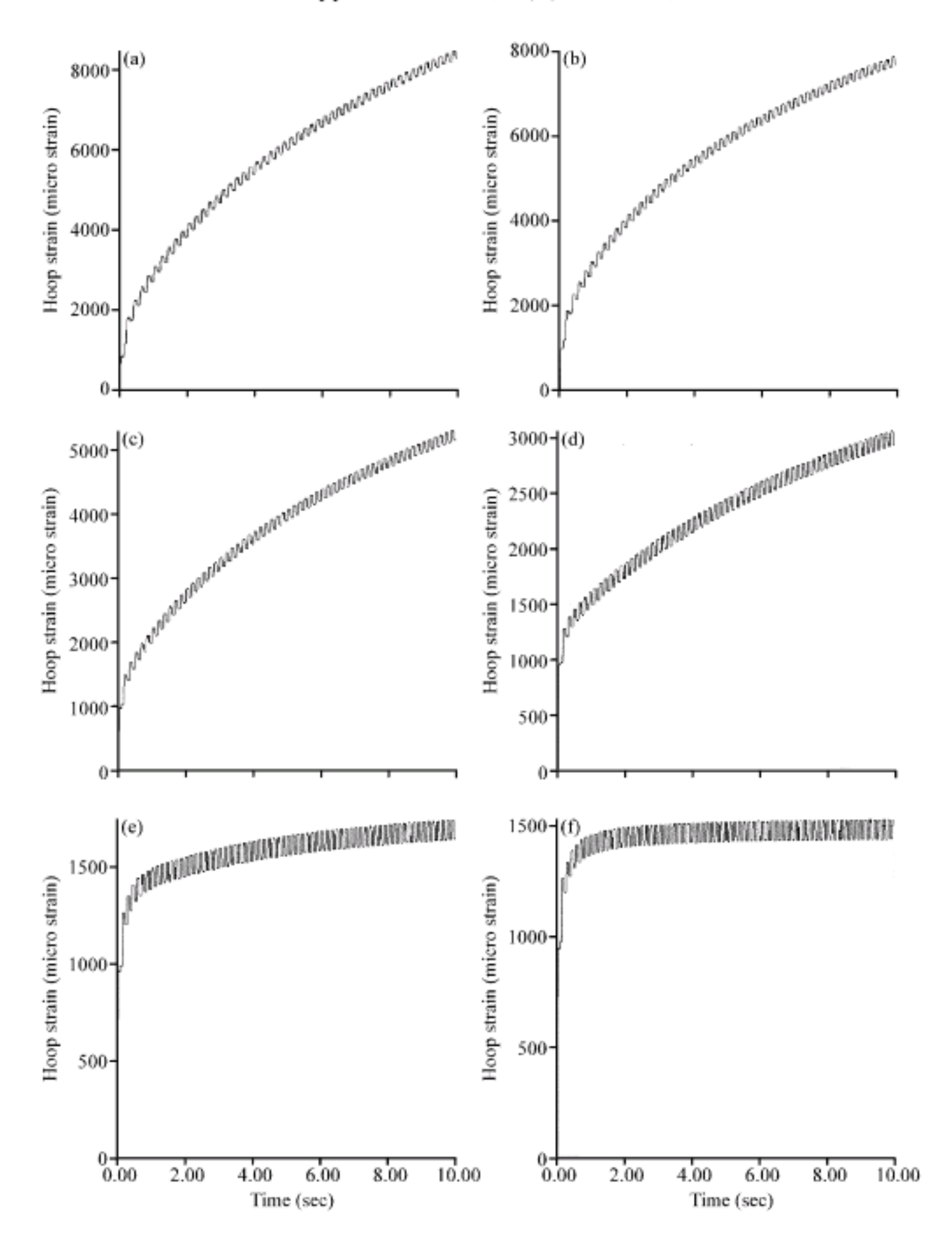


Fig. 9: Hoop strain data using FE analysis for the top surface of the specimen SS at a dynamic bending moment of 724.10 Nm. (a) Frequency = 5.00 Hz; (b) Frequency = 5.50 Hz; (c) Frequency = 6.00 Hz; (d) Frequency = 6.50 Hz; (e) Frequency = 7.00 Hz and (f) Frequency = 7.25 Hz

Table 4: FE (combined) ratchet rate averaged over the first 10 sec for specimen SS (με/cycle)

Frequency (Hz)	Dynamic bending moment (Nm)				
	582.45	632.45	680.10	724.10	
5.00	14.25	17.55	30.67	170.17	
5.50	12.57	14.59	19.06	143.32	
6.00	11.40	13.08	17.28	87.97	
6.50	10.60	11.85	14.63	46.94	
7.00	9.86	10.98	13.13	24.41	
7.25	9.57	10.67	12.67	20.74	

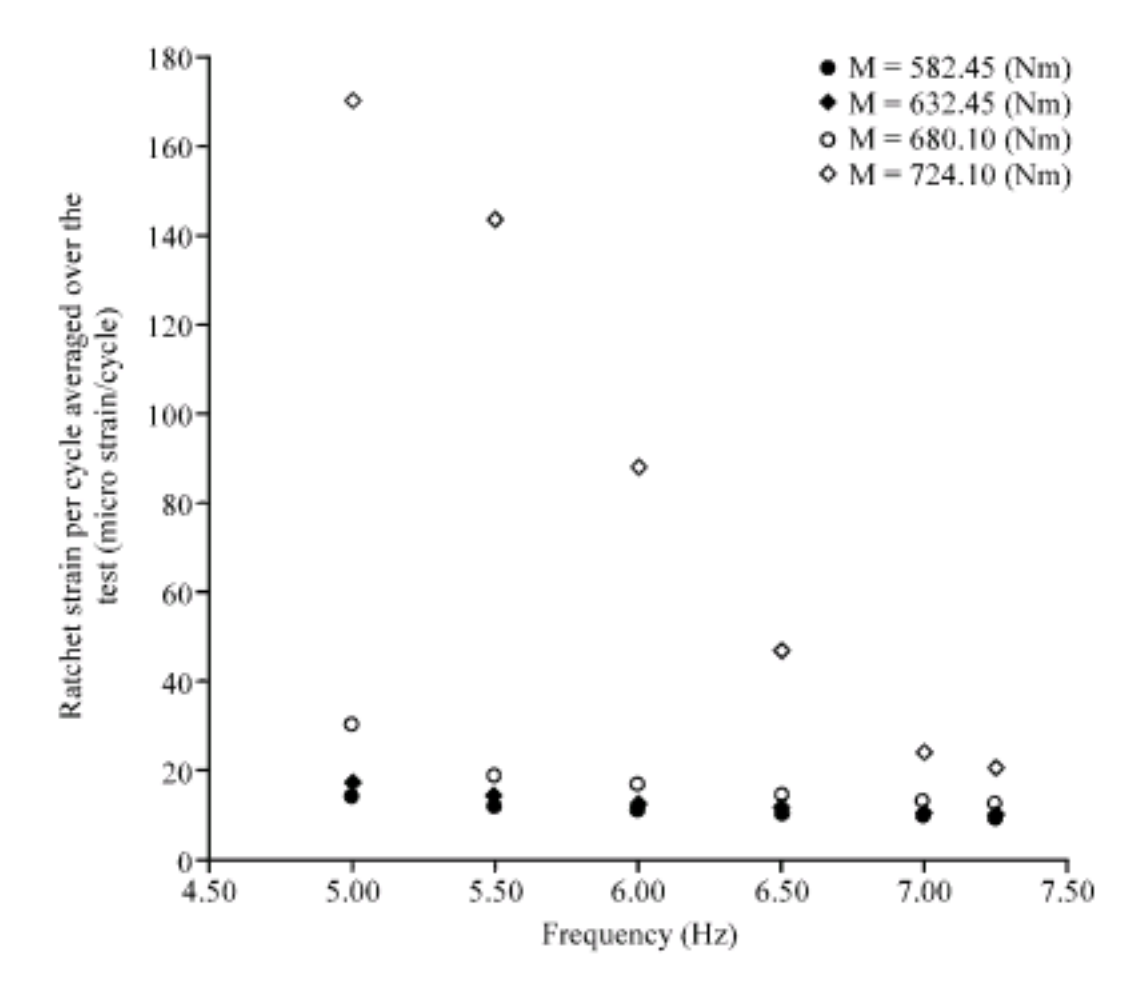


Fig. 10: The effect of frequency on the ratchetting behavior of the specimen SS

Table 5: FE (combined) hoop strain over the first 10 sec for specimen SS (με)

Frequency (Hz)	Dynamic bending moment (Nm)				
	582.45	632.45	680.10	724.10	
5.0	712.72	877.67	1533.73	8508.51	
5.5	690.17	801.03	1046.61	7868.06	
6.0	686.14	787.58	1040.29	5295.67	
6.5	688.77	770.86	950.84	3050.78	
7.0	689.89	768.98	919.01	1708.81	
7.25	694.59	774.71	920.19	1505.89	

Data obtained for $P = P_d = 26.10 \text{ MPa}$ (P/P_{0.2} = 0.66). $M_{0.2}$ was based on proof stress $\sigma_{0.2} = 242 \text{ MPa}$

RESULTS AND DISCUSSION

The experimental work reported here provides reliable data which can be used to judge the value of FE analysis using the ABAQUS package. However, it should be noted that the experimental work used a rising amplitude technique which may effectively reduce the ratchet strain at any particular dynamic bending moment. It is possible that those tests conducted at low amplitude will harden the material sufficiently to reduce the ratchet strains observed at higher amplitudes. It is not possible to quantify the possible magnitude of this effect. This possible effect would not have influenced the dynamic bending moment at which ratchetting was first observed. Typical data obtained experimentally and from FE model for specimen SS on the average of the top and bottom surface are shown in Fig. 6.

Both experimental results and the FE analysis agree that ratcheting is influenced by the material stress-strain curve and load history. The rate of ratchetting depends significantly on the magnitudes of the internal pressure, dynamic bending moment and material constants for combined hardening model. The results show that initially, the calculated rate of ratchetting is large and then decreases with the increasing of cycles. The FE model predicts the hoop strain ratchetting rate to be near that found experimentally in all cases that $M/M_{P0.2} \le 1$. Otherwise, the results show that the FE method gives over estimated values comparing with the experimental data.

The linear kinematic model is a simple model that gives only a first approximation of the behavior of metals subjected to cyclic loading, as explained in above. The nonlinear isotropic/kinematic hardening model can provide more accurate results in many cases involving cyclic loading, but it does have several limitations. For example, the model dictates that the governing isotropic hardening equation is independent of the strain range. Experimental results have shown that the amount and rate of isotropic hardening may depend on the magnitude of the strain range. Thus, it is recommended that the model be calibrated with experimental data that is close to the expected strain range and loading history of the application. Therefore, it is important to accurately calibrate the plasticity model to experimental data in such a way to distinguish the individual contributions of isotropic and kinematic hardening to the overall material response. The results obtained from FE method based on the present model comparing with previous work (Zehsaz *et al.*, 2008) to be near that found experimental data.

Also, the results of FE analysis in Table 4, 5 and Fig. 9, 10 show that when the bending moment is constant then the hoop strain ratchetting decreases with the increasing of frequency and far away from the resonant frequency value. The maximum hoop strain ratchetting occurs at proximity the resonant frequency value. For specimen SS, the resonant frequency is about 5 Hz. In Table 3 by increasing the dynamic bending moment in constant frequency, the hoop strain ratchet rate increases. Otherwise, the hoop strain ratchetting extremely increases in the resonant frequency with the increasing of the dynamic bending moment. Of course, in frequencies far away from the resonant frequency value the effect of increasing the bending moment is less than increasing the hoop strain ratchetting. The relative increasing rate of hoop strain ratchetting is 11% for frequency = 5Hz and dynamic bending moment from 582.45 to 724.10 Nm. Otherwise, it considers that the hoop strain ratchet rate is 1% in frequency = 7.26 Hz and the same dynamic bending moment range.

ACKNOWLEDGMENTS

Appreciation is expressed to the technical staff of the Applied Mechanics Division of the Department of Mechanical Engineering at the University of Tabriz (Iran) for their assistance with the work.

NOTATIONS

t : Cylinder thickness
 D_m : Cylinder mean diameter
 D₀ : Cylinder outside diameter

E : Young's modulus

M : Dynamic bending moment

M_y : Yield moment

M_{P0.2}: 0.2% collapse moment
 P: Internal pressure
 P_d: Design pressure
 P_v: Yield pressure

S_m: Allowable design stress intensity
y: Thickness correction factor = 0.4

 σ_{ult} : Tensile stress σ_{v} : Yield stress

f : Yield surface

J₂ : Von-Misses yield function

σ : Stress tensor

σ' : Stress deviatoric tensor

X : Back stress tensor

X': Back stress deviatoric tensor
 k: Initial size of the yield surface
 R: Isotropic hardening parameter

b, Q: Materials constants for isotropic hardening
 C,γ: Materials constants for kinematic hardening

ε^P : Plastic strain tensor ε_P : Equivalent plastic strain

REFERENCES

- Abdel-Karim, M. and N. Ohno, 2000. Kinematic hardening model suitable for ratcheting with steady-state. Int. J. Plasticity, 16: 225-240.
- Abdel-Karim, M., 2005. Numerical integration method for kinematic hardening rules with partial activation of dynamic recovery term. Int. J. Plasticity, 21: 1303-1321.
- Armstrong, P.J. and C.O. Frederick, 1966. A mathematical representation of the multi axial Bauschinger effect. CEGB report RD/B/N 731, Central Electricity Generating Board. The report is reproduced as a paper: 2007. Materials at High Temperatures, 24: 1-26.
- Bari, S. and T. Hassan, 2001. Kinematic hardening rules in uncoupled modeling for multi axial ratcheting simulation. Int. J. Plasticity, 17: 885-905.
- Bari, S. and T. Hassan, 2002. An advancement in cyclic plasticity modeling for multi axial ratcheting simulation. Int. J. Plasticity, 18: 873-894.
- Beaney, E.M., 1990. Failure of pipe work subjected to seismic loading. Nuclear Electric International Report, TD/B/6315/R90.
- Beaney, E.M., 1991. Measurement of dynamic response and failure of pipe work. Strain, 27: 88-94.
- Cao, J., W. Lee, H.S. Cheng, M. Seniw, H.P. Wangc and K. Chung, 2009. Experimental and numerical investigation of combined isotropic-kinematic hardening behavior of sheet metals Int. J. Plasticity, 25: 942-972.
- Chaboche, J.L., 1989. Constitutive equations for cyclic plasticity and cyclic viscoplasticity. Int. J. Plasticity, 5: 247-302.
- Chaboche, J.L., 1991. On some modifications of kinematic hardening to improve the description of ratcheting effects. Int. J. Plasticity, 7: 661-678.
- Chaboche, J.L., 1994. Modeling of ratcheting: Evaluation of various approaches. Eur. J. Mech. A Solids, 13: 501-518.
- Chaboche, J.L., 2008. A review of some plasticity and viscoplasticity constitutive theories. Int. J. Plasticity, 24: 1642-1963.
- Chen, X. and R. Jiao, 2004. Modified kinematic hardening rule for multi axial ratcheting prediction. Int. J. Plasticity, 20: 871-898.
- Chen, X., R. Jiao and S.K. Kwang, 2005. On the Ohno-Wang kinematic hardening rules for multi axial ratcheting modeling of medium carbon steel. Int. J. Plasticity, 21: 161-184.
- English, W.F., 1988. Piping and fitting dynamic reliability program-fourth semi-annual progress report. Nov. 1986-Apr. 1987, GE Nuclear Energy, NEDC- 31542.

- Eslami, M.R. and H. Mahbadi, 2001. Cyclic loading of thermal stress. J. Thermal Stress, 24: 577-603.
- Johansson, G., M. Ekh and K. Runesson, 2005. Computational modeling of inelastic large ratcheting strains. Int. J. Plasticity, 21: 955-980.
- Lemaitre, J. and J.L. Chaboche, 1994. Mechanics of Solid Materials. Cambridge University Press, Cambridge, pp: 584.
- Moreton, D.N., K. Yahiaoui, D.G. Moffat, H.C. Machin and L.A. Amesbury, 1994. The behavior of pressurized plain pipe work subjected to simulated seismic loading. Strain J. BSSM., 30: 63-71.
- Moreton, D.N., K. Yahiaoui, D.G. Moffat and M. Zehsaz, 1996. The effect of diameter/thickness ratio on the ratchetting behavior of pressurized plain pipe work subjected to simulated seismic loading. Strain J. BSSM, 32: 91-96.
- Moreton, D.N., M. Zehsaz, K. Yahiaoui and D.G. Moffat, 1998a. Ratchetting of plain pressurized pipe work subjected to dynamic bending moments: Design code implications. Seismic Engineering: ASME, Pressure Vessels Conf. Sandiago, 364: 83-98.
- Moreton, D.N., M. Zehsaz, K. Yahiaoui and D.G. Moffat, 1998b. The ratchetting of plain carbon steel pressurized cylinders subjected to simulated seismic bending: The effect of the D/t ratio and component with finite element predictions. J. Strain Anal., 33: 39-53.
- Prager, W., 1956. A new method of analyzing stresses and strains in work-hardening plastic solids. J. Applied Mech., 23: 493-496.
- Rahman, S.M., T. Hassan and E. Corona, 2008. Evaluation of cyclic plasticity models in ratcheting simulation of straight pipes under cyclic bending and steady internal pressure. Int. J. Plasticity, 24: 1756-1791.
- Ranganath, S., H. Hwang and S.W. Tagart, 1989. Piping and fitting dynamic reliability program. EPRI Nuclear Power Division.
- Tasnim, H., T. Lakhdar and K. Shree, 2008. Influence of non-proportional loading on ratcheting responses and simulations by two recent cyclic plasticity models. Int. J. Plasticity, 24: 1863-1889.
- Touboul, F., N. Blay, P. Sollogoub and S. Chapuliot, 2006. Enhanced seismic criteria for piping. Nucl. Eng. Design, 236: 1-9.
- Zehsaz, M., S.J. Zakavi, H. Mahbadi and M.R. Eslami, 2008. Cyclic strain accumulation of plain stainless steel pressurized cylinders subjected to dynamic bending moment. J. Applied Sci., 8: 3129-3138.